

Failure mechanism and soil deformation pattern of soil beneath interfering square footings

Arash Alimardani Lavasan* Mahmoud Ghazavi**

ARTICLE INFO

Article history:

Received:

January 2014.

Revised:

July 2014.

Accepted:

October 2014.

Keywords:

Footing interference,
failure mechanism,
deformation pattern,
ultimate bearing
capacity, square footing,
finite difference method,
FLAC 3D.

Abstract:

In this research, the variation of ultimate bearing capacity, failure mechanism and deformation pattern of soil beneath two closely square footings have been studied using numerical methods. It is assumed that the adjacent footings are constructed on the surface of sand. The presented numerical analyses are based on explicit-finite-difference code, *FLAC^{3D}*. The elasto-plastic behavior of soil is modeled by using Mohr-Coulomb failure criteria along with associated flow rule for the soil. The reliability of constructed numerical simulation is investigated using available data on interfering footings. In addition, a large scale test is performed on two closely spaced square footings. Failure mechanism and deformation pattern are compared with the results obtained from numerical data. A pretty well agreement is observed between numerical and experimental results. The numerical analyses have shown a significant influence of interference on the failure mechanism and deformation pattern of the soil as well as the footing ultimate bearing capacity.

1. Introduction

Comprehensive theoretical methods are available for calculating ultimate bearing capacity of square footings. Despite this fact, the subject is still of significant interest to researchers. An important shortcoming in existing methods is that there is almost no clear achievement on the failure mechanism and deformation pattern of the soil beneath the square footing. For instance, Terzaghi (1943)[23] presented a shape factor to calculate the ultimate bearing capacity of single square footing on the basis of strip failure mechanism. Other famous theoretical methods of estimating the bearing capacity [11,18,24] followed the same postulation for evaluating the characteristics of non-strip foundations. They presented the shape factor on the basis of semi-empirical modifications of a strict solution applied to a strip footing over a weightless half-space. The exact behavior of square footing is not considered in

the process of calculating ultimate bearing capacity by traditional methods. Recently, some analytical approaches are attempted to estimate the behavior of single square footings. Saran et al. (2006)[21] suggested an analytical method on the basis of normal and shear stress distribution at downward and outward of square and rectangular footings. They obtained the values of normal and shear stresses using the theory of elasticity. Fig. 1 shows the pattern of shear and normal stresses outward the length of footing (L) used by Saran et al. (2006)[21]. They assumed that the locus of points of maximum shear stresses (Y_0) varied with respect to moving zones geometry at a given depth (z).

Saran et al. (2006)[21] also performed some experimental tests and expressed that the presented analytical method led to reasonable results.

Golder (1941)[9] evaluated the failure mechanism of square footing placed on granular sand. He presented the collapse mechanism on the soil surface and beneath square footing as showed in Fig. 2.

*Corresponding Author : PhD , Civil Engineering Department , K.N. Toosi University of Technology, Tehran Iran. Email :a_alimardani@dena.kntu.ac.ir

** Professor, Civil Engineering Department, K.N. Toosi University of Technology, Tehran, Iran. Email :ghazavi_ma@kntu.ac.ir

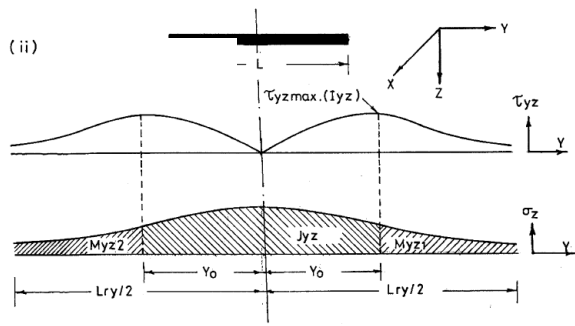


Fig.1: The pattern of soil shear and normal stress beneath footing (Saran et al., 2006)

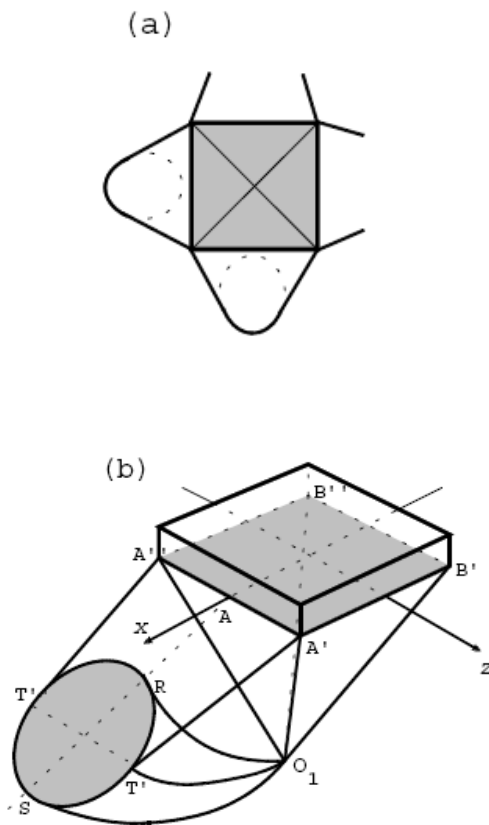


Fig. 2: Collapse mechanism in the depth and surface of soil beneath square footing [9]: a) Collapse pattern on soil surface; b) view of collapse pattern

As seen in Fig. 2, the failure mechanism is symmetric around x and z axes. Golder (1941)[9] stated that the tetrahedral block immediately placed beneath the footing moved down and four surrounding flanks were separated from the soil non-linearly in a cone shape. Michalowski (2001)[19] modified the abovementioned pattern to a multi block mechanism and found the limit loads by using upper-

bound calculation method. He considered four plane-strain regions. He concluded that this conventional mechanism led to least upper bound solution.

With rapid innovation in computational efforts in recent decade, the numerical modeling became more customary with respect to the capabilities of numerical methods in processing failure and collapse mechanism developed in soil beneath footings. Michalowski and Dawson (2002)[20] investigated the accuracy of numerical analysis for limit loads imposed on square footings using FLAC3D software. They compared the numerical results with those obtained from kinematic approach for limit load [19] and traditional theoretical equations [11,18,23,24]. The analyses were conducted by considering the Mohr-Coulomb failure criteria obeying associated flow rule. According to the results of this study, the difference between upper bound approach and numerical limit load analysis increases by increasing the internal friction angle of the soil. The results related to prior method were permanently lower. Michalowski and Dawson (2002)[20] showed that the limit loads calculated on the basis of kinematic upper bound were significantly overestimated. Fig. 3 shows the velocity contour of the soil around rigid-rough square footing expressed by Michalowski and Dawson (2002)[20].

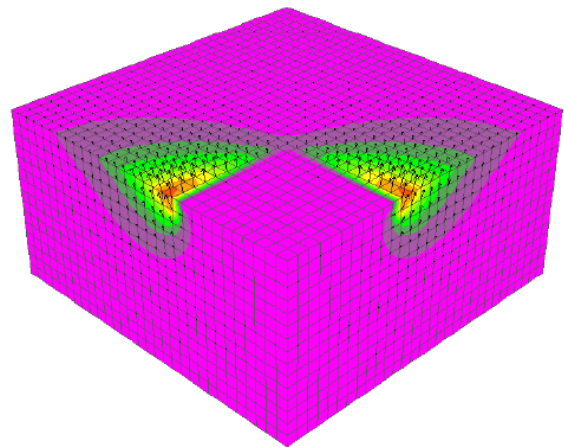


Fig. 3: Velocity contours in neighborhood of a rough square footing (Michalowski and Dawson, 2002[20])

They also revealed that numerical analysis by FLAC3D led to more reasonable results in comparison with kinematic approach of limit load. From their point of views the overestimation of upper bound approach is related to the strict assumption of plane-strain deformation.

All above research works focus on isolated footings. In some practical situations, two footings may be located close to each other. This results in more complicated patterns of failure and deformation. No information is found on the variation of mechanism of failure occurred in the soil beneath two interfering square footings at various spacings. Stuart (1962)[22], Das and Larbi-Cherif

(1983)[2], Kumar and Saran (2003)[15], Ghazavi and Lavasan (2007, 2008)[7,8] studied the influence of interference on the ultimate bearing capacity of closely spaced strip and square footings. All these studies indicate that the interaction between two neighboring footings result in increasing the ultimate bearing capacity. Stuart (1962)[22] introduced the dimensionless efficiency factors ($\xi\gamma$ and ξq) as the ratio of ultimate bearing capacity of interfering footings to the ultimate bearing capacity of the same isolated footing on the same granular material.

A comprehensive numerical study has been conducted on the variation of soil deformation pattern and failure mechanism at various spacings between two adjacent square footings. The reliability of numerical simulation of two adjacent footings, several verification analyses are performed and the results are compared with those obtained from existing experimental data. Due to the uncertainty of failure mechanism of the soil beneath interfering square footings reported by the previous researchers, the numerical results of failure mechanism obtained for interfering strip footings are compared with those of analytical studies.

2. Numerical Analysis Procedure

The numerical simulation of two closely spaced square footings is performed using commercially available finite difference code, FLAC3D (Itasca Group, 2001). The stress-strain behavior of the soil is predicted on the basis of Mohr-Coulomb failure criteria obeying a non-associated flow rule. Non-associativity of soil is considered by assuming different values for the internal friction angle and dilation angle of the soil. The analyses are conducted based on displacement control.

The rigid square footings are assumed to be fully rough. The rigidity of footings is simulated by prescribing an equal displacement to the nodes of the soil exactly beneath the footing base. Therefore, the footing structure is not modeled directly. The roughness of footing is simulated by constraining a horizontal displacement of the soil nodes at the bottom of footings. Due to the symmetry of soil-footing system, only a quarter of the system is simulated in the numerical simulation. To avoid the influence of the boundaries on the numerical analysis, the nodes at the vertical boundaries are allowed for planar movement. The nodes at the bottom are also prescribed for zero vertical displacement. Some earlier studies showed that the magnitude of applied displacement in each step (velocity) had a significant influence on the numerical bearing capacity calculated by FLAC3D [6,8]. In present study, the sensitiveness of ultimate bearing capacity to applied

velocity is investigated by a number of trial analyses. The results of these analyses illustrated that the numerical ultimate bearing capacity was dependent on the velocities greater than $3e-5$. Thus, the magnitude of the applied velocity is assumed as $1e-6$ m/step.

The effect of boundaries on the collapse load, deformation pattern and failure mechanism of the soil beneath interfering square footings having a width of B is eliminated by taking the dimension of the model equal to $7B$ beyond the footings edges in both horizontal and vertical directions. Former studies on the calculation of ultimate bearing capacity determined from FLAC analysis showed that the mesh pattern had a significant effect on the results [6,17]. These studies have shown that accurate results are mostly obtained by considering a uniform and fine grid distribution beneath and around footings, respectively. Fig. 4 shows the typical mesh pattern for the square footing at center to center spacing between footings (Δ) equal to $2B$.

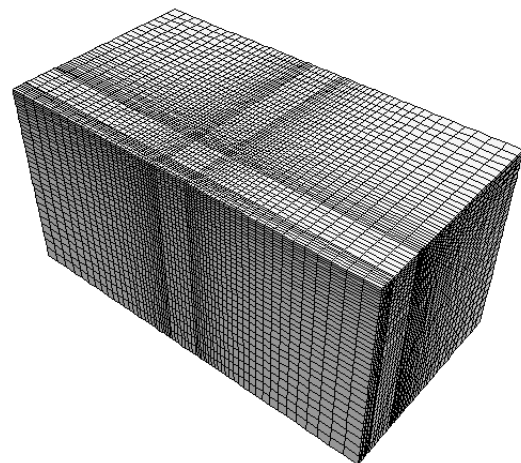


Fig. 4: Typical mesh pattern and grid-point distribution for two closely spaced square footings ($\Delta/B=2$)

3. Mechanical Behavior and Parameters of Soil and Verification Analyses

Stress-strain behavior of soil is calculated using elastic perfectly plastic Mohr-Coulomb failure criteria accompanied with non-associative flow rule. [1,3,4,6,10,12,14,25,26,27] have shown that considering Mohr-Coulomb yield condition leads to reasonable results for numerical analysis of shallow foundation on granular soils. Such assumption is used in the present study, due to the simplicity of stress path and static condition of loading. According to significant influence of soil dilation angle value, some trial analyses

are performed in this study to investigate the effect of dilation angle (ψ) on the bearing capacity and failure mechanism of soil beneath square footing. The results indicated that for soil friction angle in the range of 30° to 40° , assigning the soil dilation angle in the range of $1/2\phi \leq \psi \leq 2/3\phi$ gives reasonable results which are in good agreement with experimental data.

To ensure the reliability of the numerical simulation of square footings on granular sand, a comprehensive verification analysis is performed on existing experimental and empirical studies conducted on the bearing capacity and failure mechanism of interfering footings.

Stuart (1962)[22] presented a theoretical method for calculating bearing capacity factors of two closely spaced strip footings on non-cohesive soils on the basis of a proposed failure mechanism. Fig. 5 shows the failure mechanism proposed by Stuart (1962)[22] and its variation with spacing between two neighboring footings.

As shown in Fig. 5, the interaction between adjacent neighboring footings leads to a significant variation in the soil beneath interfering footings. At narrow spacings, the failure zones below footings merge to each other towards the inner side between two footings and cause a significant enlargement in the size of failure zones at the outer sides of each footing. This behavior increase significantly the ultimate bearing capacity of interacting footings. The variations of efficiency factor ($\xi\gamma$) at different spacing ratio (Δ/B) are presented for the soil with friction angle in the range of $30^\circ \leq \phi \leq 40^\circ$.

Das and Larbi-Cherif performed an experimental study on ultimate bearing capacity of interfering strip footings. The footings dimensions were 50.8×304.8 mm resting on granular sand with the unit weight and friction angle of 15.88 kN/m³ and 38° , respectively.

Kumar and Saran (2003)[15] studied the ultimate bearing capacity of interfering strip and square footings on non-cohesive soil. The soil was assumed as poorly graded sand (SP) with friction angle of 37° at $Dr=60\%$. The dimensions of strip footings used in the above research work were 10×86 cm.

Kumar and Ghosh (2007)[13] conducted an analytical method to predict the variation of ultimate bearing capacity of closely spaced strip footings on the basis of a possible mechanism. Their proposed mechanism is solved based on equilibrium method. Fig. 6 shows the variation of failure mechanism proposed by Kumar and Ghosh (2007)[13] for the soil with friction angle of 30° . As seen, this variation is typically resembled with those suggested by Stuart (1962)[22].

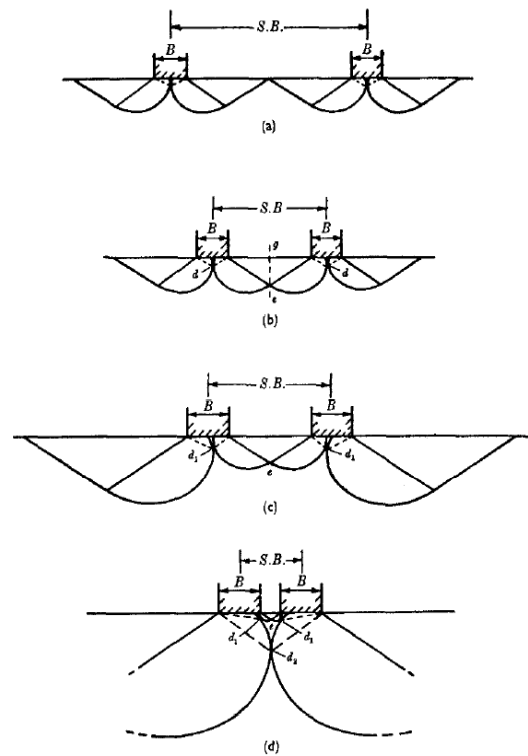


Fig. 5: Failure mechanism in soil beneath two adjacent strip footings (Stuart, 1962)[22]

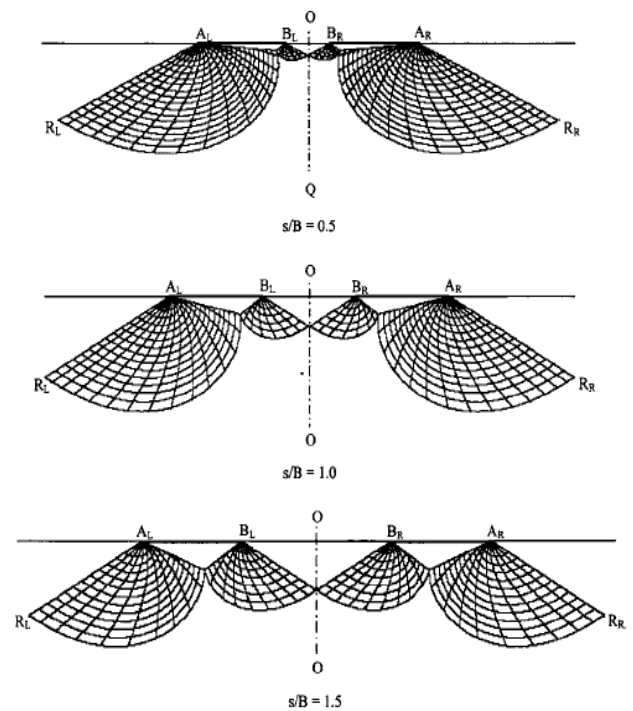


Fig. 6: The failure mechanism in soil beneath two adjacent strip footings proposed by Kumar and Ghosh (2007)[13]

In order to investigate the accuracy of numerical modeling, some verification analyses were performed by numerical simulation of laboratory tests performed by Das and Larbi-Cherif (1983)[2] and Kumar and Saran (2003)[15]. The results obtained from numerical analysis for the ultimate bearing capacity of interfering footings are compared with those of experiments. The predicted failure mechanism and its variation regime are analogized with those proposed by Stuart (1962)[22] and Kumar and Ghosh (2007)[13].

In the current analyses, the mechanical properties of the soil are presented in Table 1.

Table.1: Mechanical properties of sand in numerical modeling

Research	γ_d (kN/m ³)	K (kPa)	G (kPa)	ϕ (deg.)	ψ (deg.)	c (kPa.)
Das and Larbi-Cherif (1983)[2]	15.9	12,000	6,200	38	18	0.1
Kumar and Saran (2003)[15]	16	11,100	4,600	37	20	0.1
Present study (square footings)	15.5	10,000	4,000	34	17	0.1

Fig. 7 shows the variation of the efficiency factor (ξ_γ) versus Δ/B determined from FLAC3D analyses and the analytical solution of Stuart (1962)[22], Kumar and Ghosh (2007)[13], as well as the experiments conducted by Das and Larbi-Cherif (1983)[2] and Kumar and Saran (2007)[15].

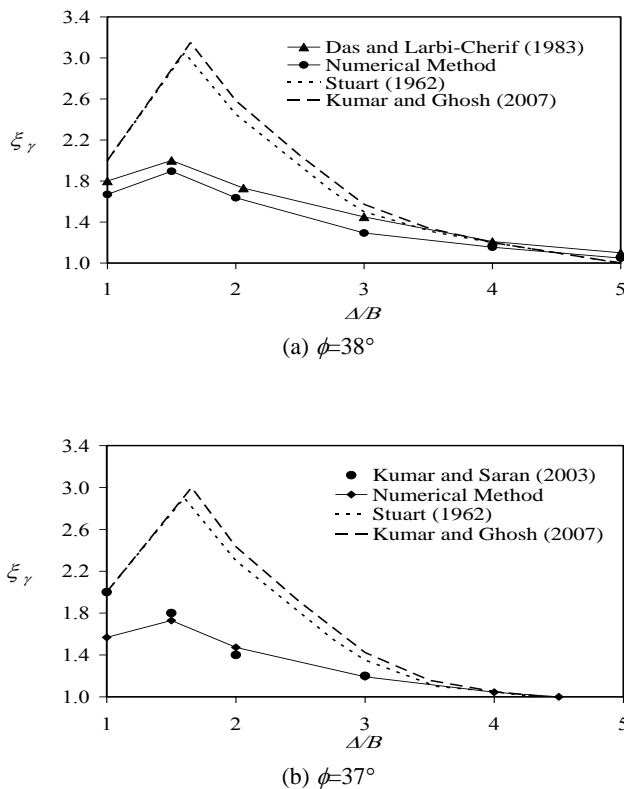


Fig. 7: Comparing the numerical, analytical and experimental efficiency factor ξ_γ

According to Fig. 7, theoretical methods has significantly over-predicted the values of efficiency factor (ξ_γ). The numerical values for efficiency factor ξ_γ are in excellent agreement with experimental data for both $\phi=37^\circ$ and 38° .

The reasonable conformation of numerical and experimental ultimate bearing capacity of interfering footings confirm that the assumptions such as mesh pattern, initial and boundary conditions, mechanical parameters of material, and fixity

conditions considered for numerical analyses are reasonable and further analyses are warranted.

The numerically acquired failure mechanisms are almost identical to the abovementioned experimental studies due to similarity of used soil. Fig. 8 and 9 show the soil deformation pattern and shear failure mechanism, respectively, obtained from numerical simulation of Das and Larbi-Cherif research work. According to these figures, a single failure mechanism is developed when two neighboring strip footings are placed exactly beside each other. The same single failure mechanism underneath two footings is observed for $\Delta/B=1.5$. It means that for center to center spacing values between two adjacent strip footings less than $1.5B$, two footings and the soil between them act as a single footing with the width of $B+\Delta$. Therefore, a unique failure zone is formed in larger dimension beneath the system. This phenomenon, called blocking, increases significantly the ultimate bearing capacity. For spacing greater than $\Delta=1.5B$, the size of deformation pattern and failure mechanism begin to shrink. According to Figs. 8 and 9, for $\Delta/B>2$, the interacting failure mechanisms are developed beneath each footing separately. For all these spacing ratios, although the system of failure mechanism is symmetric, the failure and deformation patterns are asymmetric underneath each footing. This asymmetry is due to the interaction of two footings at near spacing. By increasing the distance between two neighboring footings, the failure zones are changed into symmetrical shape. At $\Delta=6B$, the deformation pattern and failure mechanism are identical to those expected for an isolated strip footing.

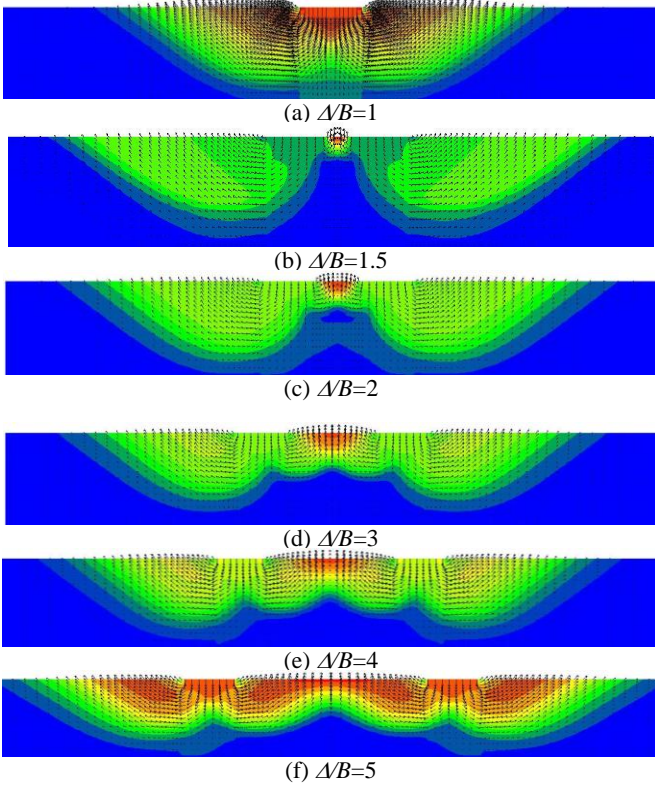


Fig. 8: Displacement contours and vector for interfering strip footings at various spacing ratios ($\phi=38^\circ$)

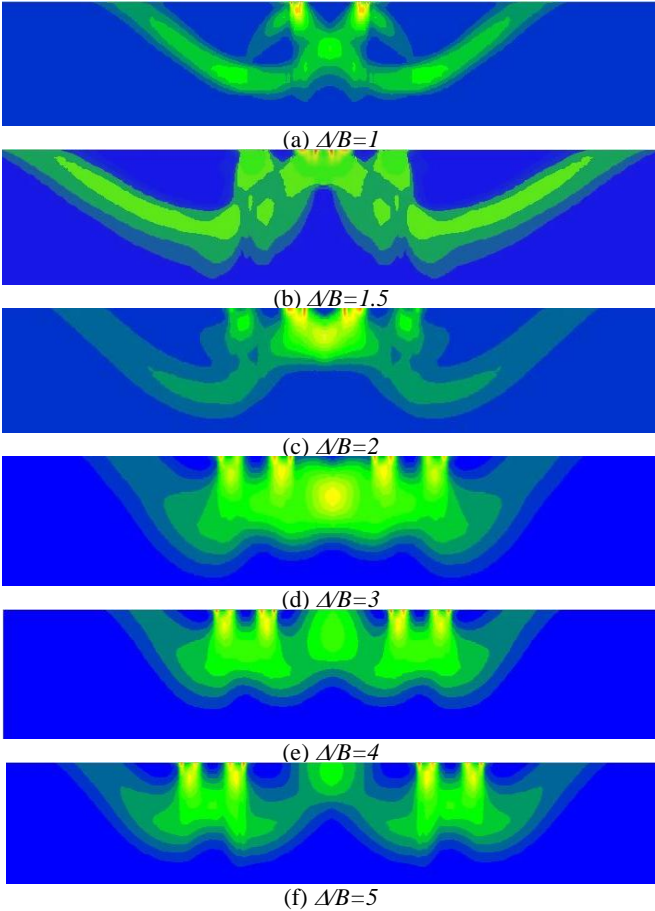


Fig. 9: Shear strain rate contours for interfering strip footings at various spacing ratios ($\phi=38^\circ$)

Comparing Figs. 8 and 9 with Figs. 6 and 7 states that a fairly satisfactory agreement between analytically expected and numerically obtained failure mechanism beneath two closely spaced strip footings. The conformity of results indicates the reliability of the numerical modeling in predicting the failure mechanism at interference occurrence.

4. Behavior of Interfering Square Footings

In this section, ultimate bearing capacity and failure mechanism of closely spaced square footings are investigated on the surface of cohesionless soils using numerical modeling. Table 1 presents the mechanical parameters of soil used in the numerical simulation of interfering square footings. The dimensions of interfering square footings are assumed as 40×40 cm.

The efficiency factor (ξ_γ) for closely spaced square footings are defined as:

$$\xi_\gamma = \frac{q_{u(\text{interfering})}}{q_{u(\text{single})}} \quad (1)$$

where q_u (interfering) is ultimate bearing capacity of interfering square footings and q_u (single) is ultimate bearing capacity of isolated square footings.

Fig. 10 shows the variation of efficiency factor (ξ_γ) obtained from numerical analysis for two adjacent square footings at different spacing values.

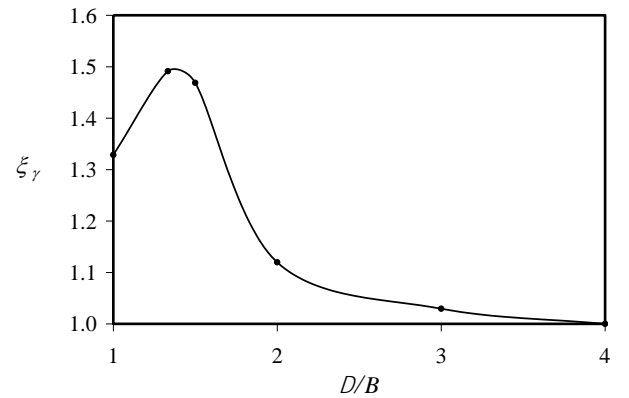


Fig. 10: Variation of efficiency factor (ξ_γ) at various spacing for interfering square footings

According to Fig. 10, the blocking occurs when center to center spacing between two neighboring footings is in the range of $\Delta \leq 1.3B$. Therefore, the efficiency factor value increases by increasing the spacing between footings in this range. The efficiency factor begins to decrease in greater

spacing ratios. The interference has no influence on the ultimate bearing capacity when the spacing is about $4B$.

Figs. 11 and 12 shows the variation of soil deformation patterns around and beneath two closely constructed square footings, respectively. As seen in Fig. 11, the deformation patterns are similar to the one expected for an isolated rectangular footing when two square footings are placed beside each other $\Delta=B$. At this spacing ratio, the deformation pattern is significantly developed in y-y direction in comparison with the x-x direction. By increasing the spacing between two adjacent footings up to $1.3B$, the same distribution is observed in the deformation pattern at soil surface. The concentration of displacement at soil surface increases in x-x direction by increasing the spacing between footings. This means that the behavior of closely spaced square footings is similar to that of single rectangular footing at low spacing. This resemblance is disappeared by an increase in spacing. As seen in Fig. 11, the displacement field at soil surface approaches towards that of expected for an isolated square footing. Besides, the interference has no effect on the deformation pattern for center to center spacing greater than $4B$.

As shown in Fig. 12, the soil deformation pattern in x-x direction at low spacing is more significant comparing to y-y direction. The influenced depth of soil due to footing loading is greater in x-x direction than y-y direction.

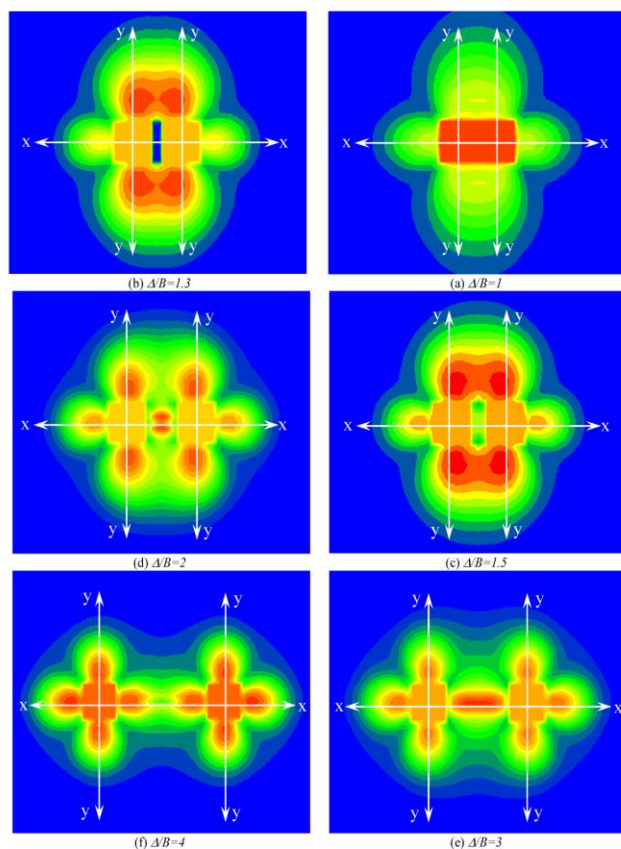


Fig. 11: Displacement contours of interfering square footings at soil surface

According to Fig. 12, the soil in the middle of two footings is rigidly resists against the downward moving of footings. This behavior occurs for $\Delta \leq 1.5B$ regarding a significant increase in passive forces acting on this confined zone. The soil unrestrainedly moves in that area due to decreasing of passive force on the confined zone between neighboring footings. The size of deformed zone tends to decrease in y-y direction by increasing the spacing between two adjacent square footings. The trend of deformation size variation in y-y direction is opposite to that of x-x direction.

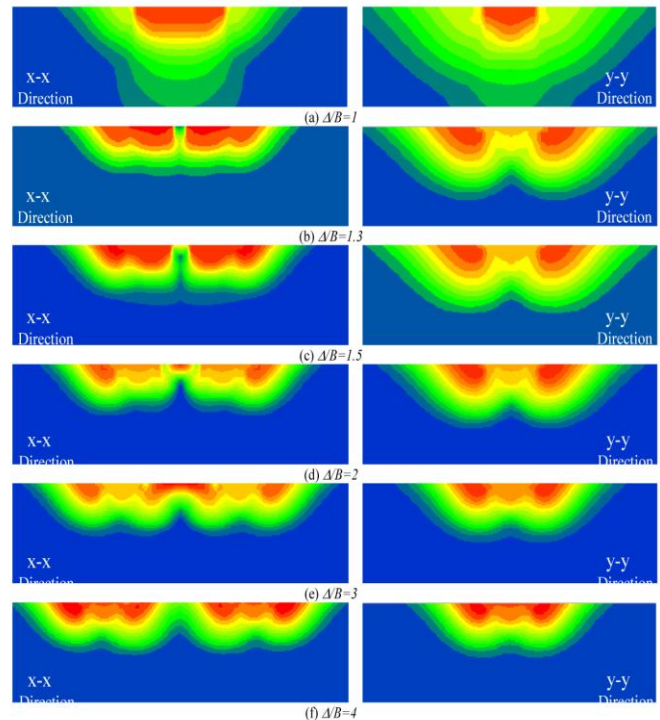


Fig. 12: Displacement contours of soil beneath interfering square footings

When the deformations, developed in soil beneath footings, are equal in x-x and y-y directions, the effect of interference is vanished. Such behavior is observed at $\Delta/B=4$.

For more clarification in soil failure mechanism of interfering square footings, the variation of shear strain rate contours are presented in Figs. 13 and 14 for the surface and depth of soil, respectively.

According to Fig. 13, the failure mechanism at soil surface is exactly similar to that of single rectangular footing at $\Delta \leq 1.5B$. It can be revealed that in this spacing range, two closely spaced footings behave like an isolated rectangular footing with a width of B and length of $B+\Delta$. In such cases, the soil between footings works as an elastic rigid block and therefore the shear bands cannot be developed due to the highly concentrated confining stress in this zone. Such treatment was expected with respect to deformation pattern at this spacing range. As seen in Fig. 13, at closer center to

center spacing, the shear bands are considerably extended in y-y direction rather than x-x direction. By increasing the spacing, the size of shear band decreases in y-y direction and increases in x-x direction. The interference has no effect on the failure mechanism when the shear bands in both directions have the same shapes and sizes. This approach is observed at soil surface by considering the center to center spacing almost equal to $4B$. According to Fig. 13, the width and length of affected zone from edges of footings are about $2.5B$ and $1.5B$ in y-y and x-x directions, respectively, when two footings are placed exactly beside each other. At center to center spacing ratios in the range of $\Delta \leq 2B$, the size of failure pattern decreases to about $2.2B$ and $1.2B$ in the width (y-y direction) and length (x-x direction), respectively.

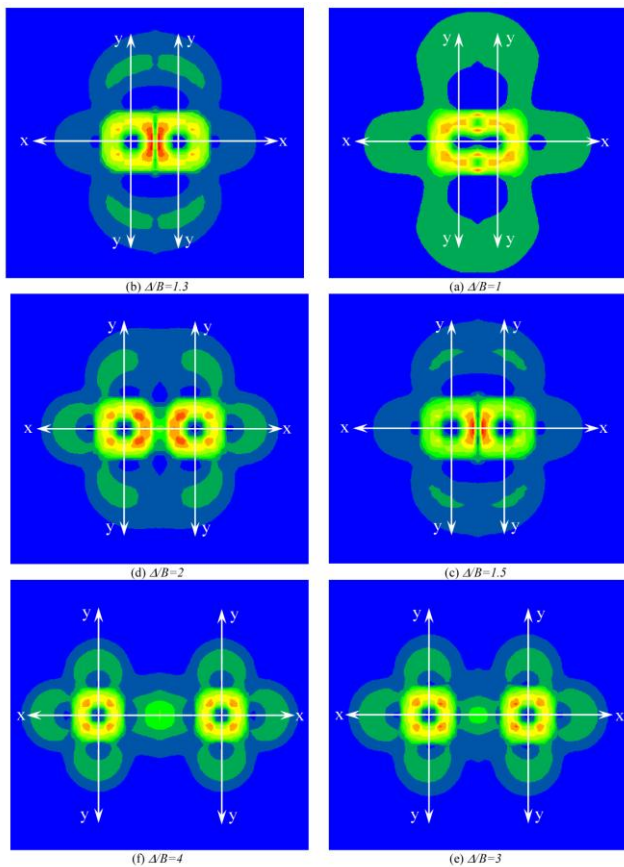


Fig. 13: Strain rate contours of interfering square footings at soil surface

Regarding Fig. 13, at wide spacing values ($\Delta \geq 4B$), the size of failure mechanism becomes symmetric about x-x and y-y directions. At this condition, the width and length of failure pattern are approximately $1.2B$ in both directions. The maximum depth of failure zones is almost $2.5B$ in y-y direction and $2B$ in x-x direction at $\Delta=B$. An increase in spacing between square footings results in the decrease of influenced depth in y-y direction which is contrary to that of x-x direction.

At wide spacing ($\Delta \geq 4B$), the depth of failure mechanism is developed in the depth about $1.8B$. This value is observed for an isolated square footing on identical sandy soil.

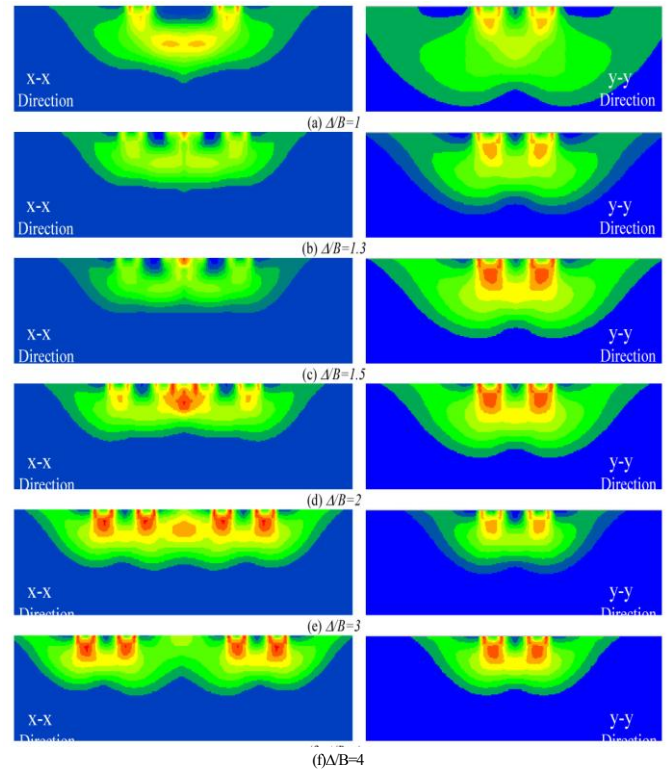


Fig. 14: Strain rate contours of soil beneath interfering square footings

5. Conclusion

Ultimate bearing capacity, soil deformation pattern and failure mechanism for two closely spaced square footings are investigated using numerical analysis based on finite difference FLAC3D software. The results of numerical modeling of interfering square footings show that the interference causes significant increase in the ultimate bearing capacity up to 1.5 times than that obtained for an isolated identical footing. The ultimate bearing capacity is maximum at $\Delta/B=1.3$ which is the maximum spacing of blocking occurrence. The influence of interference on the ultimate bearing capacity is eliminated at center to center spacing greater than $3B$. The variation of failure mechanism and deformation pattern of soil indicates that the failure is developed in the direction perpendicular to the interference axis (x-x direction). At close spacing, the width, length and depth of failure zone and deformation in y-y direction are significantly greater than those generated in the other direction. Therefore, it is found the failure in the direction perpendicular to the interference axis is more crucial. The disappearance of the influence of interference on failure mechanism leads to develop the failure mechanism with identical shape and size in x-x and y-y directions.

References

- [1] Bolton, M. D., and Lau, C. K., 1993. Vertical bearing capacity factors for circular and strip footings on Mohr-Coulomb soil. *Canadian Geotechnical Journal*, 30, pp. 1024–1033.
- [2] Das, B.M., and Larbi-Cherif, S. 1983. Bearing Capacity of Two Closely Spaced Shallow Foundations on Sand. *Soils and Foundations*, 23(1), pp. 1-7.
- [3] De Borst, R., and Vermeer, P.A. 1984. Possibilities and Limitations of Finite Elements for Limit Analysis. *Geotechnique*, 34(2), pp. 199-210.
- [4] Erickson, H.L., and Drescher, A. 2002. Bearing Capacity of Circular Footings. *Journal of Geotechnical and Geoenvironmental Engineering*, ASCE, 128(1), pp. 38-43.
- [5] FLAC-Fast Lagrangian Analysis of Continua, Version 2.1., 2001. ITASCA Consulting Group, Inc., Minneapolis.
- [6] Frydman, S., and Burd, H.J. 1997. Numerical Studies of Bearing Capacity Factor N_γ . *Journal of Geotechnical and Geoenvironmental Engineering*, ASCE, 123(1), pp. 20-29.
- [7] Ghazavi, M., and Lavasan, A.A., 2007. Influence of Interference on Bearing Capacity of Strip Footing on Reinforced Sand. In *Proceedings of 5th International Symposium on Earth Reinforcement*, pp. 431-436, Fukuoka, Japan.
- [8] Ghazavi, M., and Lavasan, A.A., 2008. Interference effect of shallow foundations constructed on sand reinforced with geosynthetics. *Geotextiles and Geomembranes*, vol. 26, pp. 404-415.
- [9] Golder H.Q., 1941. The ultimate bearing pressure of rectangular footings. *Journal of the Institution of Civil Engineers*, 17(2), pp. 161–174.
- [10] Griffiths, D.V., 1982. Computation of bearing capacity factors using finite elements. *Geotechnique*, 32(3), pp. 195-202.
- [11] Hansen, B.J., 1970. A Revised and Extended Formula for Bearing Capacity. Danish Geotechnical Institute Copenhagen, Denmark. Bul., No. 28, pp. 21.
- [12] Hjjaj, M., Lyamin, A.V., Sloan, S.W., 2004. Numerical Limit Analysis Solutions for the Bearing Capacity Factor N_γ . *International Journal of Solids and Structures*, vol. 42, pp. 1681-1704.
- [13] Kumar, J., and Ghosh, P. 2007. Ultimate Bearing Capacity of Two Interfering Rough Strip Footings. *Journal of Geotechnical and Geoenvironmental Engineering*, ASCE, 7(1), pp. 53-62.
- [14] Kumar, J., Kouzer, K.M., 2007. Bearing capacity of two interfering footings, *International Journal for Numerical and Analytical Methods in Geomechanics*. DOI: 10.1002/nag.625
- [15] Kumar, A., and Saran, S. 2003. Closely Spaced Footings on Geogrid-Reinforced Sand. *Journal of Geotechnical and Geoenvironmental Engineering*, ASCE, 129(7), pp. 660-664.
- [16] Lee, J., and Salgado, R. 2005. Estimation of Bearing Capacity of Circular Footings on Sands Based on Cone Penetration Test. *Journal of Geotechnical and Geoenvironmental Engineering*, ASCE, 131(4), pp. 442-452.
- [17] Lee, J., Salgado, R., and Kim, S. 2005. Bearing Capacity of Circular Footings under Surcharge Using State-Dependent Finite Element Analysis. *Computers and Geotechnics*, vol. 32, pp. 445-457.
- [18] Meyerhof, G.G., 1952. The Ultimate Bearing Capacity of Foundations. *Geotechnique*, 3(2), pp. 301-332.
- [19] Michalowski R.L., 2001. Upper-bound load estimates on square and rectangular footings, *Géotechnique*, 51(9), pp. 787–798.
- [20] Michalowski, R.L., and Dawson, E.M., 2002. Three-Dimensional Analysis of Limit Loads on Mohr-Coulomb Soil. *Foundations of Civil and Environmental Engineering*. No. 1, pp. 137-147.
- [21] Saran, S., Kumar, S., Grag, K.G., and Kumar, A., 2006. Analysis of square and rectangular footings subjected to eccentric-inclined load resting on reinforced sand. *Geotechnical and Geological Engineering*, DOI: 10.1007/s10706-006-0010-7.
- [22] Stuart, J.G. 1962. Interference between Foundations with Special Reference to Surface Footings in Sand. *Geotechnique*, 12(1), pp. 15-23.
- [23] Terzaghi, K., 1943. *Theoretical Soil Mechanics*. Wiley, Inc, New York.
- [24] Vesic, A.S. 1973. Analysis of Ultimate Loads of Shallow Foundations. *Journal of Soil Mechanics and Foundations*, ASCE, 99(1), pp. 45-73.
- [25] Ukritchon, B., Whittle, A.J., Klangvijit, M., 2003. Calculations of Bearing Capacity Factor N_γ Using Numerical Limit Analyses. *Journal of Geotechnical and Geoenvironmental Engineering*, ASCE 129 (6), pp. 468-474.
- [26] Woodward, P.K., and Griffiths, D.V., 1998. Observations on the computation of the bearing capacity factor N_γ by finite elements. *Geotechnique*, 48(1), pp. 137-141.
- [27] Yin, J.H., Wang, Y.J., and Selvadurai, A.P.S., 2001. Influence of Nonassociativity on the Bearing Capacity of a Strip Footing. *Journal of Geotechnical and Geoenvironmental Engineering*, ASCE, 127(11), pp. 985-989.